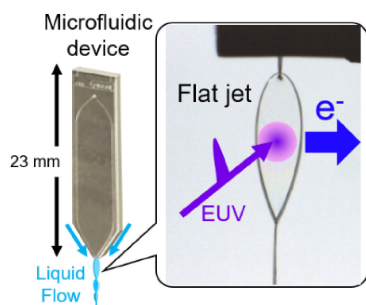


Extreme Ultraviolet Laser Photoelectron Spectroscopy of Flat Liquid Jet Generated Using Microfluidic Device

Yo-ichi Yamamoto, Hiroto Yano, Shutaro Karashima, Ryuta Uenishi,
Natsumi Orimo, Junichi Nishitani, and Toshinori Suzuki*



We have developed a microfluidic chip for liquid-liquid collisions and confirmed the generation of a thin (0.7 μm) flat liquid jet with a large cross-sectional area. The flat jet enhanced the photoelectron signal intensity by a factor of 8 compared to that for a microjet under the same laser focusing conditions, which enables quick and accurate measurement of photoelectron spectra of liquids.

REPRINTED FROM



Vol.96 No.9 2023 p.938–942

September 15, 2023

The Chemical Society of Japan

Extreme Ultraviolet Laser Photoelectron Spectroscopy of Flat Liquid Jet Generated Using Microfluidic Device

Yo-ichi Yamamoto, Hiroto Yano, Shutaro Karashima, Ryuta Uenishi, Natsumi Orimo, Junichi Nishitani, and Toshinori Suzuki*

Department of Chemistry, Graduate School of Science, Kyoto University, Kyoto 606-8502, Japan

E-mail: suzuki@kuchem.kyoto-u.ac.jp

Received: July 5, 2023; Accepted: July 29, 2023; Web Released: August 4, 2023



Toshinori Suzuki

TS received a Doctor of Science from Tohoku University in 1988. He joined the Institute for Molecular Science (IMS) as a technical associate in 1988 and became a research associate in 1989. From 1990 to 1992, he conducted research at Cornell University and UC Berkeley as a JSPS Postdoctoral Fellow for Overseas Research. In 1992, he was appointed at IMS as an associate professor and started his research group. He moved to RIKEN in 2001 as Chief Scientist and Director of the Chemical Dynamics Laboratory, and since 2008 he has been a full professor of chemistry at Kyoto University.

Abstract

We present photoelectron spectroscopy of liquid films generated in a vacuum with microfluidic devices based on liquid-liquid or gas-liquid collisions. The results are compared to those for a standard liquid microjet technique.

Keywords: Photoelectron spectroscopy | Microfluidics | Liquid

Molecular aggregation and chemical interactions at gas-liquid interfaces are of great importance for environmental sciences, synthetic chemistry and various other fields. The primary experimental means to study these interfaces have so far been nonlinear spectroscopic methods such as second-harmonic generation and sum-frequency generation techniques.^{1,2} On the other hand, extreme UV (EUV) photoelectron spectroscopy (PES) is also promising as a complementary approach for studying gas-liquid interfaces.³ Because the electron escape depth for a material is about 1 nm or less in the electron kinetic energy (eKE) range of 30–100 eV,^{4,5} EUV-PES provides high interfacial sensitivity. For example, EUV-PES enables in situ measurements of surface excess of solutes under vacuum conditions.⁶ Most importantly, EUV-PES provides insights into electronic structures at gas-liquid interfaces.

PES studies of volatile liquids have generally been performed using a cylindrically shaped liquid microjet $\sim 20 \mu\text{m}$ in diameter.^{7–10} The microjet can be created by discharging a liquid from a thin glass capillary or a metal aperture, which is easy to implement. However, one of the drawbacks of this technique is that the jet diameter is smaller than the typical focal spot size (100–200 μm) for a laser beam, so that the photon flux cannot be fully utilized, which limits the data acquisition efficiency. The electron escape depth is extremely small ($\sim 1 \text{ nm}$)

for a liquid, so the EUV photoelectron signal is inherently weak. Moreover, because the number density of a solute is typically three orders of magnitude smaller than that of a solvent, the signal from a solute is extremely weak. Consequently, data acquisition in time-resolved EUV-PES of a solute typically takes well over 24 h. This difficulty can be mitigated by increasing the repetition rate of the EUV laser to the sub-megahertz range using a Yb-based laser.¹¹ To further maximize the photoelectron signal, it is also important to reduce the size mismatch between the laser focal spot and the liquid target. This can be achieved by increasing the area of the liquid target for EUV-PES measurements. The liquid must travel in vacuum at high speed for the following two reasons. One is to continuously bring a fresh sample to the focal point of the laser operated at a repetition rate $> 10 \text{ kHz}$. The speed of a liquid flow must be higher than 3 m/sec to avoid two consecutive laser pulses in the 10 kHz pulse train from exciting the same portion of the liquid. Our experimental condition provides a speed higher than 20 m/sec. The other is to transport the sample liquid into the laser interaction region before extensive evaporative cooling occurs under vacuum.

There have been at least three different methods reported for generating a traveling liquid film, or a flat jet.¹² The first employs liquid-liquid collisions; two liquid microjets collide under vacuum, resulting in the merged liquid being squeezed into a thin film. This method has been implemented for soft X-ray absorption spectroscopy,¹³ high-order harmonic generation (HHG)¹⁴, soft X-ray transient absorption spectroscopy,¹⁵ and photoelectron spectroscopy.¹⁶ The second method employs a slit-shaped nozzle to discharge a liquid into a vacuum;¹⁷ a very narrow slit can be fabricated using photolithography to generate a submicron-thick liquid film.^{18,19} The advantage of this

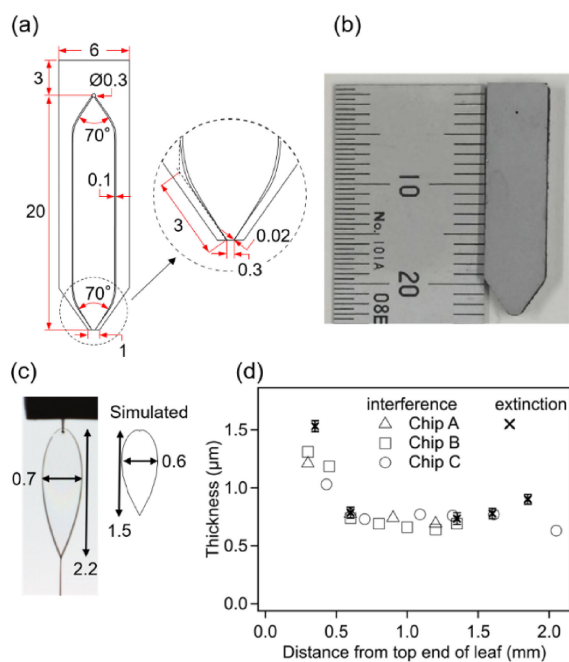


Figure 1. Microfluidic chip and flat liquid jet. (a) Design of flow channels (units: mm). The depth of the channel is 20 μm . (b) Microfluidic device made from Si (units: mm). (c) Formation of stable liquid film at flow rate of 1.5 mL/min. The simulated film shape is shown on the right-hand side (units: mm). (d) Thickness of flat liquid jet estimated using interference and extinction methods.

method is that it provides a well-defined liquid thickness that is crucial for photoabsorption spectroscopy. The third method uses gas-liquid collisions in a gas-dynamic nozzle, in which a liquid microjet is aerodynamically flattened by two gas jets impinging from opposite sides.²⁰ The advantages of this method are that the film thickness can be controlled by the gas jet pressure and that very thin films (<100 nm) can be generated using strong gas jets.

In the present study, we primarily employ the first of these three methods. However, instead of using two independent liquid microjet nozzles, we employ a single microfluidic device to discharge two precisely aligned liquid jets. This method allows liquid jets to collide precisely with each other, generating a stable liquid film over a long period of time. We fabricated a microfluidic device of our own design. In the following, we describe the performance of this device for EUV-PES measurements. We also briefly compare the results of a performance test using the third method.

We designed the flow channels based on a past study on liquid-liquid collision.²¹ Our design is shown in Figure 1(a). We chose a crossing angle of 70° between the two jets, with the liquid-liquid collision point 0.1 mm downstream from the end of the microchip. The two flow channels are mirror images of each other, which ensures a well-balanced liquid flow rate for the two microjets. The flow channels have a rectangular cross section with dimensions of $100 \times 20 \mu\text{m}$ almost entirely to prevent the pressure loss in the channels. However, the width decreases gradually from 3 mm upstream of the exits to $20 \mu\text{m}$ at the exit to increase the flow speed. The collision of high-

speed liquid jets creates a large liquid film. The outer V-shape of the chip is to avoid spatial interference with the permanent magnet and electron sampling skimmer that are placed a few millimeters away from the liquid film in the vacuum chamber. We employed photolithography to produce grooves in a Si wafer with a thickness of 1.5 mm, bonded the grooved surface of this wafer to a flat Si wafer to form enclosed channels, and then used laser-dicing to isolate individual chips. A photograph of a diced chip is shown in Figure 1(b). Each microchip was then coated with graphite to prevent charge-up. The microfluidic chip is held between a flat plate and a holder made of PEEK (polyether ether ketone). A flow channel is drilled through the holder to enable liquid supply. An O-ring is placed around the $\phi 0.3$ -mm entrance hole of the chip to connect the chip and the holder without any leak at a high liquid pressure. A $1/16''$ PEEK tube connects the inlet of the holder and an HPLC pump. An in-line filter with $2\text{-}\mu\text{m}$ pore size, positioned between the holder and the pump, removes small particles to prevent clogging in the chip. Figure 1(c) shows a photograph of a flat jet generated by this device in air. The total liquid flow rate was 1.5 mL/min. Also shown is the predicted shape based on a previously derived equation²¹ (See Supporting Information for details). The observed width of the liquid film agrees very well with the prediction, while the length is slightly larger than predicted. The film is formed as a chain of mutually orthogonal leaves (the leaf orientation varies alternately between the x and y directions, if the flow axis is z), and the first (and largest) leaf shown in Figure 1(c) was used for PES measurements. The dimensions of the first leaf were 0.3×1.0 mm for a liquid flow rate of 1.0 mL/min, and 0.7×2.2 mm at 1.5 mL/min. These dimensions are much larger than the laser focal spot size. Figure 1(d) shows the thickness of a film measured in air for three different chips (named A–C) using white-light interferometry^{12,17} and extinction spectroscopy, the latter of which employed a dye (Rhodamine 610) solution and 532-nm light (See Supporting Information for details). These two methods provided consistent results, as seen in the plot; the thickness of the liquid film in the middle of the first leaf-shaped liquid film is $0.7 \mu\text{m}$ for a flow rate of 1.5 mL/min. The rim of a leaf is much thicker. The traveling speed of the flat liquid jet is estimated to be over 20 m/s for a total flow rate of 1.5 mL/min.

We introduced the Si chip into a photoelectron spectrometer and illuminated the first leaf with femtosecond EUV pulses to measure EUV-PE spectra. The flow rate was 1.0–1.5 mL/min. The liquid discharged into vacuum was entirely frozen in a liquid N_2 -cooled trap placed downstream. The EUV pulses were generated by HHG in Ar using the second harmonic (1 kHz, 400 nm, 0.13 mJ) of a Ti:sapphire laser.²² A single-order harmonic (EUV radiation of 27.7 eV) was selected using a time-preserving monochromator with a diffraction grating (150 grooves/mm).²³ The Si chip was held at room temperature. Since the EUV pulses also ionize gaseous water molecules evaporated from the liquid film, a negative bias voltage (-30 V) was applied to the microchip to increase the kinetic energy of photoelectrons emitted from the liquid. This enabled differentiation of the electrons emitted from the liquid and those from the evaporated gas. The photoelectrons were detected using a magnetic-bottle time-of-flight (MBTOF) electron

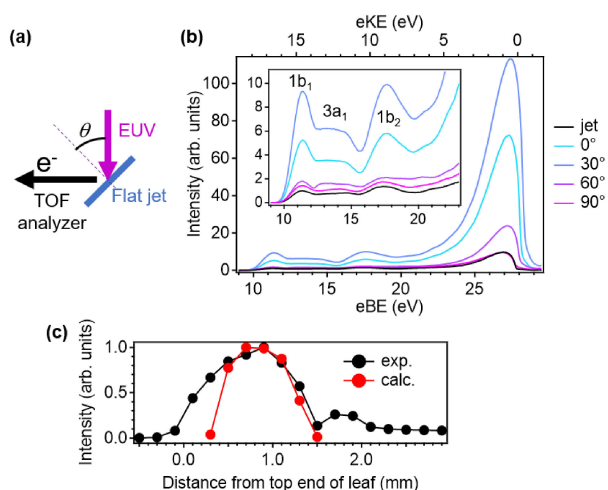


Figure 2. Photoelectron spectroscopy using flat liquid jet. (a) Geometry of experiment. (b) Photoelectron spectra of 10 mM aqueous NaI solution measured using Si microfluidic chip. A liquid flow rate of 1.0 mL/min, an excitation point 1 mm downstream from the nozzle, and various excitation-light incidence angles were employed. The black line indicates the results obtained using a microjet. The inset shows an enlarged view of the spectra, and the band assignments are indicated. Note that the rim of a liquid film is much thicker than the film itself, and an experiment at the angle of 90° illuminates the rim, providing a similar signal intensity with a microjet. (c) Dependence of signal intensity on photoexcitation position for $\theta = 30^\circ$. The expected intensities based on the leaf shape and laser spot size are indicated by red dots. The diameter of the EUV beam was 160 μm (FWHM) in these measurements.

energy analyzer²⁴ described in detail elsewhere.²⁵ The photoelectrons were guided by a diverging magnetic field provided by a permanent magnet and a solenoid coil, and introduced into the TOF analyzer through a $\phi 0.5$ -mm entrance skimmer located approximately 2 mm from the liquid. The photoelectrons were decelerated in the flight tube to enhance the resolution of the TOF analysis. The typical energy resolution was 0.1 eV, limited by the resolution of the MBTOF apparatus and the laser bandwidth. When forming a flat jet, the pressure in the main chamber and the MBTOF analyzer was 4×10^{-4} and 3×10^{-6} Torr, respectively. The temperature of the liquid film was crudely estimated to be 273–283 K based on a recent study by Chang et al.²⁶

Measured photoelectron spectra for a 10 mM aqueous NaI solution are presented in Figure 2. As shown in Figure 2(a), the electron detection axis and the EUV propagation direction are at 90° to each other. As shown in Figure 2(b), we varied the relative angle θ by rotating the flat jet and found that the intensity was maximized at around 30°. However, the angular dependence is rather moderate, and one can obtain reasonably high intensities also at 40° and 45°. The signal intensity thus achieved was 8 times higher than that obtained with a liquid microjet 25 μm in diameter. The horizontal axes in Figure 2(b) are eKE and electron binding energy (eBE), the latter of which is the difference between the photon energy and eKE. The spectra clearly reveal valence photoelectron bands associated

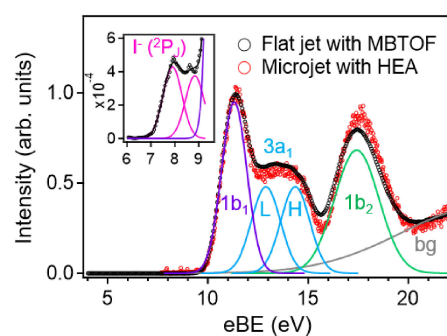


Figure 3. Photoelectron spectra of 50 mM aqueous NaI solution. Black circles: flat jet combined with MBTOF spectrometer and EUV laser. The ionization point was 0.6 mm downstream from the microchip and θ was 40°. The inset shows an enlarged view of the energy region for iodide anions. Solid lines indicate the decomposition of the valence bands. A broad background photoelectron signal is indicated as bg. Red circles: microjet combined with HEA and He(II) radiation.

with liquid water, such as 1b₁ (HOMO) and 3a₁ (HOMO-1). The strong peak at low eKE is due to electrons inelastically scattered and decelerated in the liquid, which is unavoidable for PES of liquids. Figure 2(c) shows the dependence of the photoelectron signal intensity on the downstream position, with θ fixed at 30°. The results are in reasonable agreement with the expected values.

Due to insufficient durability of the Si chip, we proceeded to fabricate a similar chip using borosilicate glass and further evaluated the utility of this device in EUV-PES. We performed EUV-PES of NaI aqueous solutions at 40.0 eV, which is close to the energy of He(II) radiation (40.8 eV). The time-preserving monochromator (500 grooves/mm) provided good spectral isolation of 40.0 eV radiation (13th harmonic); the measured contamination from 21.6 (7th harmonic), 27.7 (9th harmonic) and 33.9 eV radiation (11th harmonic) was 4.8, 2.4 and 1.4%, respectively. Figure 3 presents EUV-PE spectra of a 50 mM NaI solution obtained using our present instrument, together with that²⁷ obtained using a hemispherical electron energy analyzer (HEA, Gamma-data Scienta SES 100) and He(II) radiation (electron cyclotron resonance light source) with a liquid microjet in our laboratory.²⁸ The two spectra are seen to be in reasonable agreement with each other. The agreement with HEA, which has a higher instrumental resolution, ensured a sufficiently high accuracy of the laser-MBTOF method combined with the liquid film. Small differences are attributed in part to the influence of photoemission anisotropy: our MBTOF spectrometer collects photoelectrons emitted at all angles, while the HEA has a finite solid angle for electron detection. Another possible source of the difference is that the negative bias voltage employed in the present study (−36 V) was not sufficiently high to completely remove the signal associated with gaseous water. In the case of the HEA, the bias voltage was −70 V, so that spectral contamination from gaseous water could be completely neglected.^{27,29} Using the cut-off energy method, we estimated the eBE for the water 1b₁ band to be 11.3 eV, in excellent agreement with values reported in the literature.^{30,31} The eBE values for the 3a₁L, 3a₁H, and 1b₂

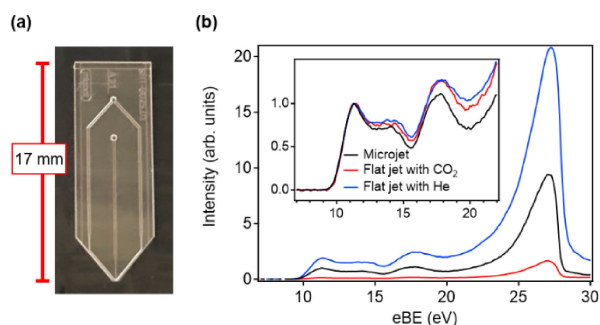


Figure 4. Photoelectron spectroscopy using gas-dynamic microfluidic chip. (a) Photograph of commercial microfluidic device employed for measurements. (b) Comparison of EUV photoelectron spectra of 10 mM NaI aqueous solution measured using three different methods. For the flat jets, the ionization point was 0.3 mm downstream from the nozzle and θ was 45° . The probe photon energy was 27.7 eV. The inset shows spectra normalized by the peak intensity of the $1b_1$ band for water.

valence bands were estimated to be 12.9, 14.4, and 17.4 eV, respectively. These bands are slightly more sensitive to the underlying background electron signal. The photoelectron spectrum of I^- is also clearly seen in the inset of Figure 3. The acquisition time for the spectrum using a 5 kHz EUV laser was 10 min, while measurements using the HEA and He(II) radiation took at least 1.5 h.²⁷ The high data acquisition efficiency is an advantage of EUV-PES using a laser-MBTOF method and the flat jet further improves the efficiency.

For comparison, spectra were also acquired for flat liquid jets obtained using a gas-dynamic nozzle, for which a commercial microfluidic chip is available (Micronit Inc., Figure 4(a)). The chip is made of borosilicate glass, and has a central channel with cross-sectional dimensions of $30 \times 20 \mu\text{m}$ for liquid flow, and two side channels with dimensions of $60 \times 50 \mu\text{m}$ for gas flows. The crossing angle between the liquid microjet and gas jets is 40° . Because the colliding gas considerably increases the local pressure above the liquid film, this type of nozzle seems unfavorable for application to PES. However, we considered that it may be of use with He as a colliding gas, because He has no internal degrees of freedom that would otherwise cause rovibrational inelastic scattering of electrons. The total electron scattering cross-section for He is less than $4 \times 10^{-16} \text{cm}^2$ at 10 eV.³² Figure 4(b) shows a comparison of EUV photoelectron spectra for flat jets obtained using a gas-dynamic nozzle with He or CO_2 as the colliding gas, and a standard liquid microjet 25 μm in diameter. It can be seen that the flat jet with He gas exhibited almost the same features at that for the microjet. The spectral intensity obtainable using a gas-dynamic nozzle with He is about two times higher than with a standard microjet, while it is four times smaller than with the liquid-liquid collision nozzle. In contrast, when CO_2 is used as the colliding gas, the spectral intensity is about one order of magnitude smaller than that for the microjet. This reduction in intensity is attributed to the larger electron scattering cross-section for CO_2 ($>13 \times 10^{-16} \text{cm}^2$ at 10 eV).^{33,34} The gas dynamic nozzle inevitably increases electron scattering in the gas phase, generating a stronger background signal that peaks at a low electron

kinetic energy (high electron binding energy). The background signal extends down to an eBE region of 20 eV, as seen in the inset of Figure 4. For the gas-dynamic nozzle, the liquid flow rate was 0.3 mL/min, which was much smaller than that for the liquid-liquid collision nozzle. However, the size of the liquid films generated by the gas-dynamic nozzle was rather small: $0.17 \times 0.50 \text{ mm}$ with He (0.45 MPa) and $0.21 \times 0.46 \text{ mm}$ with CO_2 (0.24 MPa).

In summary, we tested a microfluidic chip made of Si for liquid-liquid collisions and generated a thin (0.7 μm) liquid film with a large cross-sectional area. We also fabricated a similar chip from borosilicate glass for higher chemical durability. The performance as a film generating device is independent of the material. The flat jet thus generated enhanced the photoelectron signal intensity by a factor of about 8 compared to that for a microjet under the same laser focusing conditions. An EUV-PE spectrum of a NaI aqueous solution at 40.0 eV was measured in 10 min using a MBTOF spectrometer, an EUV laser, and a flat jet. We also found that a gas-dynamic nozzle is useful for photoelectron spectroscopy with He as the colliding gas. Time-resolved PES measurements using flat jets are currently underway in our laboratory.

This work was supported by a JSPS KAKENHI Grant (No. 21H04970, 22K14646), Mitsubishi Foundation and Toyota Riken Scholar Program. We thank Kazuki Maeda for experimental assistance and Shunsuke Adachi for valuable advice.

Supporting Information

Prediction of shape of flat liquid jets and measurements of thickness of liquid films. This material is available on <https://doi.org/10.1246/bcsj.20230151>.

References

- 1 Y. R. Shen, *Fundamentals of sum-frequency spectroscopy*. Cambridge University Press, Cambridge, **2016**.
- 2 G. L. Richmond, *Chem. Rev.* **2002**, *102*, 2693.
- 3 M. Faubel, in *Photoionization and Photodetachment*, ed. by C.-Y. Ng, World Scientific Publishing Co. Pte. Ltd., **2000**, Vol. 1, pp. 634–690.
- 4 A. Jablonski, C. J. Powell, *J. Phys. Chem. Ref. Data* **2020**, *49*, 033102.
- 5 Y.-I. Suzuki, K. Nishizawa, N. Kurahashi, T. Suzuki, *Phys. Rev. E Stat. Nonlin. Soft Matter Phys.* **2014**, *90*, 010302.
- 6 C. W. West, J. Nishitani, C. Higashimura, T. Suzuki, *Mol. Phys.* **2021**, *119*, e1748240.
- 7 M. Faubel, B. Steiner, J. P. Toennies, *J. Chem. Phys.* **1997**, *106*, 9013.
- 8 T. Kondow, F. Mafune, *Annu. Rev. Phys. Chem.* **2000**, *51*, 731.
- 9 B. Winter, M. Faubel, *Chem. Rev.* **2006**, *106*, 1176.
- 10 K. R. Wilson, B. S. Rude, J. Smith, C. Cappa, D. T. Co, R. D. Schaller, M. Larsson, T. Catalano, R. J. Saykally, *Rev. Sci. Instrum.* **2004**, *75*, 725.
- 11 Y. Miura, Y. Yamamoto, S. Karashima, N. Orimo, A. Hara, K. Fukuoka, T. Ishiyama, T. Suzuki, *J. Am. Chem. Soc.* **2023**, *145*, 3369.
- 12 M. Kondoh, M. Tsubouchi, *Opt. Express* **2014**, *22*, 14135.
- 13 M. Ekimova, W. Quevedo, M. Faubel, P. Wernet, E. T. J.

Nibbering, *Struct. Dyn.* **2015**, *2*, 054301.

14 T. T. Luu, Z. Yin, A. Jain, T. Gaumnitz, Y. Pertot, J. Ma, H. J. Wörner, *Nat. Commun.* **2018**, *9*, 3723.

15 A. D. Smith, T. Balciunas, Y. P. Chang, C. Schmidt, K. Zinchenko, F. B. Nunes, E. Rossi, V. Svoboda, Z. Yin, J. P. Wolf, H. J. Wörner, *J. Phys. Chem. Lett.* **2020**, *11*, 1981.

16 S. Malerz, H. Haak, F. Trinter, A. B. Stephansen, C. Kolbeck, M. Pohl, U. Hergenbahn, G. Meijer, B. Winter, *Rev. Sci. Instrum.* **2022**, *93*, 015101.

17 G. Galinis, J. Strucka, J. C. T. Barnard, A. Braun, R. A. Smith, J. P. Marangos, *Rev. Sci. Instrum.* **2017**, *88*, 083117.

18 D. J. Hoffman, T. B. Van Driel, T. Kroll, C. J. Crissman, E. S. Ryland, K. J. Nelson, A. A. Cordones, J. D. Koralek, D. P. DePonte, *Front. Mol. Biosci.* **2022**, *9*, 1048932.

19 C. J. Crissman, M. Mo, Z. Chen, J. Yang, D. A. Huyke, S. H. Glenzer, K. Ledbetter, J. P. F. Nunes, M. L. Ng, H. Wang, X. Shen, X. J. Wang, D. P. DePonte, *Lab Chip* **2022**, *22*, 1365.

20 J. Koralek, J. B. Kim, P. Bruza, C. Curry, Z. J. Chen, H. A. Bechtel, A. A. Cordones, P. Sperling, S. Toleikis, J. F. Kern, S. P. Moeller, S. H. Glenzer, D. P. DePonte, Proc. SPIE 11038, X-Ray Free-Electron Lasers: Advances in Source Development and Instrumentation V, Prague, Czech Republic, April 1–4, **2019**, 11038S.

21 R. Li, N. Ashgriz, *Phys. Fluids* **2006**, *18*, 087104.

22 S. Karashima, Y.-I. Suzuki, T. Suzuki, *J. Phys. Chem. Lett.* **2021**, *12*, 3755.

23 F. Frassetto, C. Cacho, C. A. Froud, I. C. E. Turcu, P. Villorresi, W. A. Bryan, E. Springate, L. Poletto, *Opt. Express* **2011**, *19*, 19169.

24 P. Kruit, F. H. Read, *J. Phys. E: Sci. Instrum.* **1983**, *16*, 313.

25 N. Kurahashi, S. Thürmer, S. Y. Liu, Y. Yamamoto, S. Karashima, A. Bhattacharya, Y. Ogi, T. Horio, T. Suzuki, *Struct. Dyn.* **2021**, *8*, 034303.

26 Y. P. Chang, Z. Yin, T. Balciunas, H. J. Wörner, J. P. Wolf, *Struct. Dyn.* **2022**, *9*, 014901.

27 T. Shinno, M. S. Thesis, Kyoto University, **2020**.

28 K. Nishizawa, K. Ohshimo, T. Suzuki, *J. Chin. Chem. Soc.* **2013**, *60*, 1403.

29 S. Thürmer, T. Shinno, T. Suzuki, *J. Phys. Chem. A* **2021**, *125*, 2492.

30 N. Kurahashi, S. Karashima, Y. Tang, T. Horio, B. Abulimiti, Y.-I. Suzuki, Y. Ogi, M. Oura, T. Suzuki, *J. Chem. Phys.* **2014**, *140*, 174506.

31 S. Malerz, F. Trinter, U. Hergenbahn, A. Ghrist, H. Ali, C. Nicolas, C. M. Saak, C. Richter, S. Hartweg, L. Nahon, C. Lee, C. Goy, D. M. Neumark, G. Meijer, I. Wilkinson, B. Winter, S. Thürmer, *Phys. Chem. Chem. Phys.* **2021**, *23*, 8246.

32 D. E. Golden, H. W. Bandel, *Phys. Rev.* **1965**, *138*, A14.

33 K. R. Hoffman, M. S. Dababneh, Y. F. Hsieh, W. E. Kauppila, V. Pol, J. H. Smart, T. S. Stein, *Phys. Rev. A* **1982**, *25*, 1393.

34 Y. Itikawa, *J. Phys. Chem. Ref. Data* **2002**, *31*, 749.